Proceedings of the ASME 2012 Internal Combustion Engine Division Fall Technical Conference
ICEF2012
September 23-26, 2012, Vancouver, BC, Canada

ICEF2012-92012

A COMPARATIVE STUDY OF NO_X COMPUTATION METHODS COUPLED TO QUASI-DIMENSIONAL MODELS IN SI ENGINES.

S. M. Aithal
Mathematics and Computer Science Division
Argonne National Laboratory
Argonne, IL 60439, USA

ABSTRACT

Quasi-dimensional models are widely used in the design, development and analyses of automotive engines. Various phenomenological and empirical relations are used in these models to reduce the computational load compared to multi-dimensional models. These quasi-dimensional models have also been used to calculate NO_x, soot and HCs using various reduced chemistry/simplified models. The extended Zeldovich mechanism is widely used for finite-rate NO_x computations in these quasi-dimensional models. However, there are several simplifying assumptions in the rate equation used for the NO_x computations. This paper compares the traditional method of finite-rate NO_x computations with full finite-rate chemistry without the simplifying assumptions used in the former method. NO_x formation in a stationary engine is studied using a single zone and two-zone (burned and unburned zone) using a 6-reaction, 7-species model. A detailed comparison of the two methods of NO computation is presented. Analyses of the temporal variation of NO predicted using these two approaches is also presented.

NOMENCLATURE

A	surface area of cylinder head (m^2)
$a_{n,k}$	coefficients fits to thermodynamic data of k^{th} species
$C_{p,k}$	molar heat capacity at constant pressure of the k^{th} species (J/mole-K)
$C_{v,k}$	molar heat capacity at constant volume of the k^{th} species (J/mole-K)
$\overline{C}_p$	mixture-averaged molar specific heat at constant pressure (J/mole-K)
$\overline{C}_v$	mixture-averaged molar specific heat at constant volume (J/mole-K)
G_k	molar Gibbs free energy of the k^{th} species (J/mole)
h_{cg}	convective heat transfer coefficient W m^{-2} K
H_k	molar enthalpy of the k^{th} species (J/mole)
H_P	enthalpy of the products (J)
H_R	enthalpy of the reactants (J)
m	instantaneous mass in the engine cylinder (kg)
m_f	mass of fuel (kg)
N_{rpm}	rotational speed of the engine (rev/min)
P	pressure (N/m^2)
P_1	pressure at BDC
Q_{in}	heat input from fuel combustion (J)
Q_{loss}	heat lost from engine cylinder (J)
R_g	gas constant (J/kg-K)
R_u	universal gas constant (J/K)
S_k	molar entropy of the k^{th} species (J/mole-K)
$T(\theta)$	average cylinder temp at crank angle θ (K)
T_w	wall temperature (K)
U_k	molar internal energy of the k^{th} species (J/mole)
$V(\theta)$	instantaneous volume at crank angle θ
$x_1(\theta)$	distance of cylinder head from TDC at θ
X_k	mole fraction of the k^{th} species

GREEK SYMBOLS

γ	ratio of specific heats
θ	crank angle
ϕ	equivalence ratio
ω	engine speed (= $6N_{rpm}$ deg/sec)

ABBREVIATION

ATDC	after top dead center
BDC	bottom dead center
CAD	crank angle degrees
EOC	end of combustion
LHV	lower heating value
RHS	right hand side
SI	spark ignition

SOC start of combustion
TDC top dead center

1 INTRODUCTION

Development of robust, computationally-efficient, physics-based modeling tools can greatly aid the design/analyses and optimization of current and next-generation engines using various fuels such as natural gas and other fuel-additive blends. Several authors have studied various aspects of performance and emissions of traditional fuels and fuel-blends both experimentally and numerically [1-14]. Experimental studies are useful in validating and calibrating numerical models. Well-validated numerical models can be used to examine a wider range of operating conditions and varied fuel-additive combinations. Furthermore, they can also be used to investigate the efficacy of newer emission-reducing technologies (catalysts, EGR etc.) which are becoming increasingly important, particularly for engines running on fuels other than gasoline. NO_x computations coupled to quasi-dimensional models serve as important design/analyses tools. These NO_x computations are conducted using equilibrium assumptions [10-14], or finite-rate chemistry using the extended Zeldovich mechanism for NO_x formation with several simplifying assumptions [5-6]. This approach is referred to as simplified finite-rate chemistry in this work. There are few studies wherein full finite-rate kinetics for NO_x formation is coupled to quasi-dimensional models [7-9]. The advantages and disadvantages of each of these approaches for NO_x computations are discussed next.

Equilibrium assumptions are most appropriate when the temperature of the working fluid is above 1800-2000K (depending on various factors such as speed, load, equivalence ratios etc). These conditions usually exist near TDC ($-5 < \theta < \theta_1$) where θ_1 corresponds to a few CAD after EOC. Under these conditions, reasonable engine-out NO_x predictions can be made [15]. Equilibrium computations conducted using the procedure outlined in [15] are fast, robust and simple to integrate with quasi-dimensional codes. However, equilibrium computations conducted using the technique of minimization of the Gibbs free energy can be computationally expensive. Equilibrium chemistry calculations conducted using look-up tables as in ref. [13] can be computationally expensive and also cumbersome.

In the simplified finite-rate chemistry approach, the extended Zeldovich mechanism is used to derive a rate expression for the time-rate of change of NO concentration and is discussed in detail in [16]. (units cm^3**,** gmol, s, K)

Table **1** shows the reactions in the extended Zeldovich mechanism (units cm^3**,** gmol, s, K)

Table 1: Extended Zeldovich mechanism with rates [16]

	Reaction	$\mathbf{K_f}$	$\mathbf{K_r}$
1	$O + N_2 = NO + N$	$7.6x10^{13}E(-38000/T)$	$1.6x10^{13}$
2	$N + O_2 = NO + O$	$6.4x10^{9}$ T E(-3150/T)	$1.5x10^{9}$T E(-3150/T)
3	$OH + N = NO + H$	$4.1x10^{13}$	$2.0x10^{14}E(-23650/T)$

Based on the extended Zeldovich mechanism, the expression for the time-rate of change of NO is given by

$$\frac{d[NO]}{dt} = k_1^+[O][N_2] + k_2^+[N][O_2] + k_3^+[N][OH] - k_1^-[NO][N] - k_2^-[NO][O] - k_3^-[NO][H] \quad (1)$$

where k_i^+ represents the forward rate and k_i^- represents the backward rate for each of the reactions shown in Table 1. The rate-expression for the NO concentration derived from the extended Zeldovich mechanism is simplified using two main assumptions, namely, (a) the C-O-H system is in equilibrium and is unaffected by N_2 dissociation, (b) atomic nitrogen (N atoms) change concentration by a quasi-steady process [17]. The first assumption implies that the concentrations O, O_2, H, OH, N_2 in Eq. (1) can be approximated by their equilibrium concentrations at a given temperature and pressure, while the second assumption implies

$$\frac{d[N]}{dt} \cong 0$$

Using these assumptions Eq. (1) can be simplified to

$$\frac{d[NO]}{dt} = \frac{2R_1\left\{1-\left([NO]/[NO]_e\right)^2\right\}}{1+\left([NO]/[NO]_e\right)R_1/(R_2+R_3)} = 2\frac{R_1 N_1}{D_1} \quad (2)$$

as explained in [16],where

$$R_1 = k_1^+[O]_e[N_2]_e = k_1^-[NO]_e[N]_e$$

$$R_2 = k_2^+[N]_e[O_2]_e = k_2^-[NO]_e[O]_e$$

$$R_3 = k_3^+[N]_e[OH]_e = k_3^-[NO]_e[H]_e$$

$$N_1 = \left\{1-\left([NO]/[NO]_e\right)^2\right\}$$

$$D_1 = 1+\left([NO]/[NO]_e\right)R_1/(R_2+R_3)$$

and the subscript 'e' denotes equilibrium values.

The rate constants and equilibrium concentration of species used in evaluating Eq. (2) is usually computed using the burned gas temperature. Models used to include the effects of mixing and gradients of the burned gas temperature can significantly impact the overall NO predictions based on Eq. (2). The simplified rate expression for NO concentration (moles/cm^3) shown in Eqs. (1) and (2) are used in works such as [5-6]. Reference [6] uses an ad-hoc calibration constant for the forward rate of the first reaction shown in Table 1. The numerical value of this calibration is not explicitly discussed. The predicted values of NO presented in Ref. [6] show a large discrepancy with experimental data. The authors of ref. [6] attribute this discrepancy to the use of a single burned gas temperature. Ref. [17] presents some experimental data which shows good agreement with the prediction of the simplified NO rate model without inclusion of the effects of mixing and burned gas temperature gradients. Authors of ref. [17]

however, point out that the good agreement seen between experimental data and the simplified NO rate model is indeed fortuitous. Given these shortcomings of the simplified finite-rate chemistry approach, it would be instructive to examine the use of a full finite-rate chemistry approach to NO computations. A rate expression for the net formation of NO, similar to Eq. (1), can be written for a chosen mechanism. The concentrations of N, O, H, N_2, O_2 OH, etc. describing the source term (net production term) are computed using finite-rate expressions for each of these species without using equilibrium assumptions. The fuel combustion chemistry is considered to be infinitely fast and hence decoupled from the NO formation mechanism. The extended Zeldovich mechanism or the 6 reaction/8 species mechanism discussed in [14] shown in Table 2 can be used in the full-finite rate NO computations. Larger, more detailed NO formation mechanisms can also be used if need be, however this would lead to increased computational cost.

Table 2: NO chemistry model with reaction rate constants (units cm^3, gmol, s, K) [14]

	Reaction	**K_f**	**K_r**
1	$O + N_2 = NO + N$	1.58E14E(-38031/T) 1.63E14E(-38095/T)	3.5E13E(-166/T)
2	$N + O_2 = NO + O$	2.65E12E(-3226/T)	5.6E11E(-19317/T) 5.9E11E(-19430/T)
3	$OH + N = NO + H$	7.33E13E(-564/T)	2.02E14E(-24725/T) 1.82E14E(-24528/T)
4	$N_2O + O = 2NO$	2.9E13E(-11657/T)	7.76E14E(-30808/T) 1.15E15E(-31568/T)
5	$N_2 + O + M = N_2O + M$	1.41E13E(-9505/T)	6.2E14E(-28247/T)
6	$O_2 + M = 2O + M$	2.6E13E(-10672/T) 8.36E6E(-61162/T) 1.03E7E(-61578/T)	

In this work, we compare NO prediction using the traditional method of finite-rate NO computations using the extended Zeldovich mechanism with full finite-rate chemistry using a 6-reaction/8 species mechanism. The simplifying assumptions in the simplified finite-rate NO computations are also closely examined.

2 MATHEMATICAL FORMULATION

The numerical model used to study the compression and power stroke of a single-cylinder diesel engine is described in detail in [18]. A similar methodology was used to model a two-zone SI engine in this work. Briefly, a zero-dimensional model was used to compute temporal variation of the temperature and pressure fields during the compression and power stroke. Temporal variation of the engine pressure and temperature during the compression and power stroke can be obtained by a numerical solution of the energy equation. Effects of temperature and mixture composition on the thermophysical properties of the working fluid were included in the solution of the energy equation. Temporal variation of the thermophysical properties of all the species in the gas mixture were obtained using thermodynamic coefficients from the CHEMKIN database. Fuel combustion chemistry was modeled by a single-step global reaction. The combustion process was modeled using the well-known Wiebe function to express the mass fraction burned. The engine cycle simulation includes unburned and burned zones. The pressure in the burned and unburned zone was assumed to be the same (as determined by the overall energy balance equation). The temperature of the burned and unburned zones at each crank angle position were computed based on the mass of the burned and unburned gas respectively, using the procedure outlined in [16]. To simplify the calculations, the ratio of densities of the unburned to burned gases was assumed to be 4, as recommended in [16]. The temporal variation of the burned and unburned gas temperatures and pressure are used for the computation of species concentrations in each of the zones. Using the procedure described in [15] the equilibrium concentration of NO, O_2, N_2, O, N and OH required for the computation of Eq. (2) can be evaluated for each crank-angle (time), which in turn can be used to obtain the temporal variation of NO. The full finite-rate computation uses the time-marching procedure described in detail in [9]. Briefly, the temporal variation of the burned and unburned gas temperature is used to compute the NO formation in each of the zones. The species concentration computed at a given crank-angle is used as the initial condition for the subsequent crank-angle. In this work, there was no mixing between the burned and unburned zones. However, the effects of mixing of the gases in the burned and unburned zone can be incorporated into the model by adjusting the species concentrations of each species at the end of each crank-angle based on the mixing model used. The mathematical equations used to compute the temporal variation of the burned and unburned gases and species concentrations are described next.

2.1 Quasi-dimensional engine model

The basic equations solved are given below.

Energy Equation:

$$\frac{dP(\theta)}{d\theta} = \frac{\gamma - 1}{V(\theta)}\left(Q_{in}\frac{dx_b}{d\theta} - \frac{h_{cg}A}{\omega}(T - T_w)\frac{\pi}{180}\right) - \gamma\frac{P(\theta)}{V(\theta)}\frac{dV}{d\theta} \quad (3)$$

$$Q_{in}(\theta) = (H_P(T) - H_R(T)) \cong m_f(\theta)LHV \quad (4)$$

$$Q_{loss}(\theta) = \frac{h_{cg}A}{\omega}(T(\theta) - T_w) \quad (5)$$

The instantaneous values of volume, area, and displacement are given by the slider-crank model [18]
The convective heat transfer coefficient was expressed as

$$h_{cg} = 3.26\, D^{-0.2} P^{0.8} T^{-0.55} w^{0.8} \quad (6)$$

where D is the bore diameter and the velocity of the burned gas w is given by

$$w = c_1 S_p + c_2 \frac{V_d T_r}{p_r V_r}(P(\theta) - P_m) \quad (7)$$

Specific heats, enthalpies, and internal energy of individual species in the working fluid were computed using polynomials as follows

$$\frac{C_{p,k}}{R_u} = a_{1,k} + a_{2,k}T + a_{3,k}T^2 + a_{4,k}T^3 + a_{5,k}T^4 \quad (8)$$

$$C_{v,k} = C_{p,k} - R_u \quad (9)$$

$$H_k = \left(a_{1,k} + \frac{a_{2,k}}{2}T + \frac{a_{3,k}}{3}T^2 + \frac{a_{4,k}}{4}T^3 + \frac{a_{5,k}}{5}T^4 + \frac{a_{6,k}}{T}\right)R_u T \quad (10)$$

$$U_k = H_k - R_u T \quad (11)$$

Mixture-averaged values of specific heat of the working fluid were averaged using mole-fractions as follows.

$$\overline{C}_v = \sum_{k=1}^{K} X_k C_{v,k}; \quad \overline{C}_p = \sum_{k=1}^{K} X_k C_{p,k}$$
$$\gamma = \frac{\overline{C}_p}{\overline{C}_v} \quad (12)$$

A similar procedure was used to compute the mixture-averaged values of enthalpy and internal energy of the working fluid.
The Wiebe function was used to compute the burned mass fraction as shown below [16]

$$x_b(\theta) = \frac{m_{fb}}{m_{fT}} = \left\{1 - \exp\left\{-a\left(\frac{\theta - \theta_0}{\theta_b}\right)^{m+1}\right\}\right\} \quad (13)$$

where, θ, θ_0, θ_b are the instantaneous crank angle, the crank angle for the start of combustion, and the combustion duration, respectively. Further, m_{fb} is the fuel burned and m_{fT} is the total fuel at BDC
The burned and unburned gas temperature were obtained

$$T_b(\theta) = \frac{P(\theta)V_b(\theta)}{m_b(\theta)R_{gb}} \quad (14)$$

$$T_u(\theta) = \frac{P(\theta)V_u(\theta)}{m_u(\theta)R_{gu}} \quad (15)$$

where, the subscripts 'u' and 'b' represent unburned and burned quantities. The volume fraction of the burned gas y_b (=V_b/V) can be obtained using the following relationship [16].

$$x_b(\theta) = \left[1 + \frac{\rho_u}{\rho_b}\left(\frac{1}{y_b} - 1\right)\right]^{-1} \quad (16)$$

The average temperature of the gas in the cylinder can be obtained by

$$T(\theta) = \frac{P(\theta)V(\theta)}{m(\theta)R_g} \quad (17)$$

2.2 Simplified finite-rate chemistry model

Eq. (2) is time-marched to obtain the temporal variation of NO. Temporal variation of temperature and pressure obtained from the solution of the energy equation is used to compute the equilibrium concentrations required for the solution of Eq. (2). Details of the methodology used to obtain equilibrium concentration of any given fuel-additive air mixture are discussed in [15]. The initial NO concentration required for time-marching Eq. (2) is 2*R_1 as recommended in [16].

2.3 Full finite-rate Chemistry

The full finite-rate chemistry model solves for each species in the NO formation model without any simplifying assumptions [9]. For each crank angle, the evolution of the concentration of species k is described by the rate equation

$$\frac{dn_k}{dt} = \omega_k \quad (18)$$

ω_k is the net production rate of species k due to all the I reactions considered in a given kinetics model, computed as shown below.

$$\omega_k = \sum_{i=1}^{I} (\upsilon_{ki} q_i); (k = 1,..., K)$$
$$\upsilon_{ki} = \upsilon''_{ki} - \upsilon'_{ki} \quad (19)$$

$$q_i = k_{fi} \prod_{k=1}^{K} n_k^{\upsilon'_{ki}} - k_{ri} \prod_{k=1}^{K} n_k^{\upsilon''_{ki}} \quad (20)$$

$$k_{fi} = A_i T^{\beta i} \exp\left(\frac{-E_i}{RT}\right) \quad (21)$$

The reaction rate constant shown in Eq. (21) is computed using the unburned and burned gas temperature for a two-zone model and the average gas temperature for a single zone model.

3 METHOD OF SOLUTION

The numerical model described above was used to compute the average pressure and temperature in a single-cylinder natural gas engine described in [19]. Methane (CH_4) was used as a surrogate for natural gas in all simulations for the sake of simplicity. The procedure to obtain the cylinder pressure in a diesel engine is explained in detail in [18]. The same procedure was adapted to obtain the pressure and temperature in an SI engine using the equations described above. Briefly, for a given set of operating conditions, namely, the prescribed mass of the fuel-air mixture and temperature at BDC, Eq. (3) was solved iteratively by using (4) through (13) to obtain the pressure from $-179° < \theta < 180°$, in increments of 1°. For a given pressure at a crank angle, the burned and unburned gas temperatures were obtained by using Eqs. (14) and (15).

The engine dimensions and operating conditions used in this work were the same as those described in [19]. Table 3 shows the engine dimensions used in this work, and Table 4 shows the operating conditions.

Table 3: Engine dimensions

Bore (mm)	130
Stroke (mm)	140
Compression ratio	11:1
Length of connecting rod (mm)	260

Table 4: Operating conditions used in this work (ϕ=0.9)

Speed (rpm)	1800
Power (kW)	33
Fuel mass (g)	0.13
Air mass (g)	2.48
Spark timing	-24° CAD

The mass of fuel (methane in this case) was kept constant at 0.13 g. A Weibe function with a = -4 and m = 2 was used to describe the rate of fuel combustion (see Eq. (13)). The combustion duration (θ_b) used in Eq. (13) was chosen such that the peak pressure matched those reported in [19] and occurred at CAD 10° ATDC. The spark timing was -24° CAD. The pressure computed using this technique matches experimental data closely. As mentioned earlier, in the two-zone model, it was assumed that there was no mixing between the burned and unburned zones. The burned zone comprised of CO_2, H_2O, excess O_2 and the corresponding amount of N_2, whereas the unburned zone comprised of the unburned fraction of fuel, O_2 and N_2.

Knowing the temporal variation of temperature, pressure and composition of the burned and unburned zones, one can compute the temporal variation of species concentrations using the full finite-rate chemistry or simplified finite-rate chemistry using the equations and methodology described in Section 2.2 and 2.3. In this work, the following 19 species were considered in computing equilibrium concentrations: CH_4, O_2, CO_2, H_2O, N_2, N, O, NO, OH, H, N_2O, CO, H_2, NO_2, HO_2, CH_3, C_2H_2, C, and HCN. The full finite-rate chemistry model shown in Table 2 requires the solution of 8 species, namely, O_2, N_2, N, O, NO, OH, H and N_2O. In other words, Eq. (18) is solved for each of the 8 species mentioned above.

4 RESULTS AND DISCUSSION

This section discusses the results of the quasi-dimensional model. Additionally, NO predictions using the full finite-rate chemistry and simplified chemistry model will also be discussed. All the results presented in this paper are for the case with $\phi = 0.9$. The results and analyses reported for $\phi = 0.9$ also hold for other equivalence ratios studied in [19].

4.1 Results from the Quasi-Dimensional Model

Figure 1 shows the variation of the normalized burned and unburned zone along with the total cylinder volume as a function of crank angle. All volumes are normalized with respect to the clearance volume. At the start of combustion the volume of the unburned gas equals the total cylinder volume. As combustion proceeds, the burned gas volume rises, slowly at first during the ignition delay period, followed by a more rapid rise. It is seen that as the combustion is almost complete the unburned gas volume tends to zero while the burned gas volume tends to the total instantaneous cylinder volume, as expected.

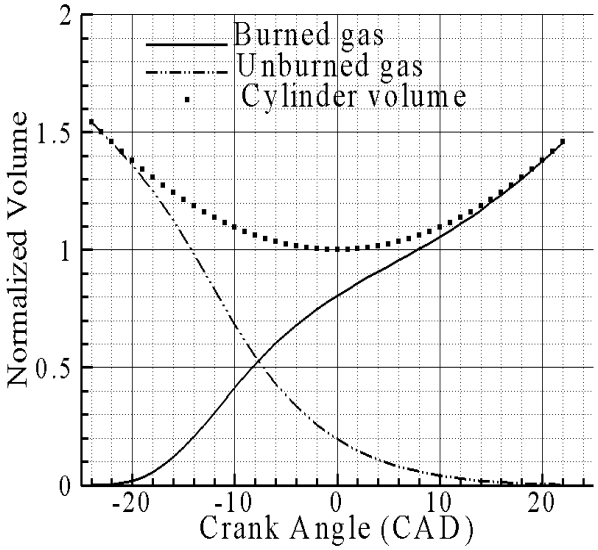

Figure 1: Temporal variation of normalized burned and unburned zone volumes.

Figure 2 shows the temporal variation of the burned and unburned gas along with the average temperature variation

obtained using a single zone model. As expected, the temperature of the unburned gas equals the single zone temperature predictions before SOC. After SOC, the burned gas temperature is considerably higher than the unburned gas temperature. After EOC, the burned gas temperature is the same as the average temperature computed using the single zone model.

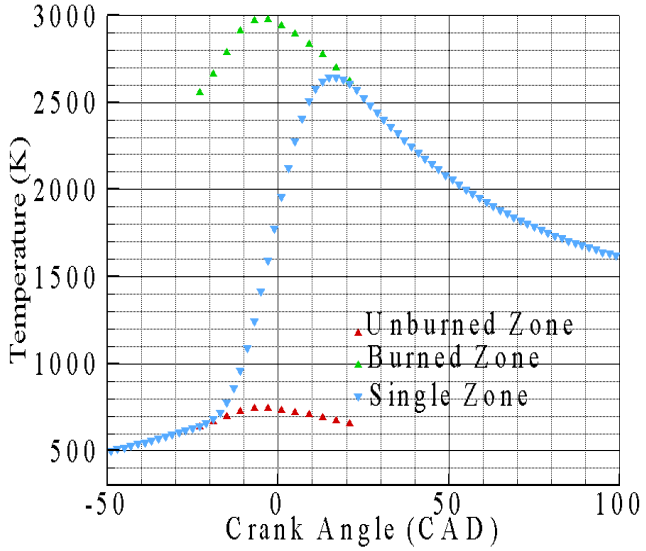

Figure 2: Temporal variation of burned and unburned gas along with the average temperature obtained from a single zone model.

Figure 3 shows the variation of normalized fuel, O_2, CO_2 and H_2O with crank-angle. All mole fractions are normalized with the value of initial fuel moles. Before SOC, the initial mixture contains 1 mole of CH_4 and 2.2 moles of O_2 along with 8.272 moles of N_2 (normalized values). Figure 3 shows that during combustion from -24 CAD to about 25 CAD, CH_4 and O_2 are depleted as dictated by Eq. (13) with the simultaneous formation of CO_2 and H_2O. As expected, after complete combustion of one mole of fuel (CH_4) with 2 moles of O_2, one mole of CO_2 and 2 moles of H_2O are formed. About 0.22 moles of O_2 remain in the burned mixed after complete combustion (since $\phi = 0.9$).

Figure 1 to Figure 3 demonstrate the correct implementation of the single zone and two-zone models used in this work. The temporal variation of temperature and pressure obtained from the single zone and two-zone models are used for computation of NO. NO predictions using the simplified chemistry model and the full-finite rate chemistry models are discussed next.

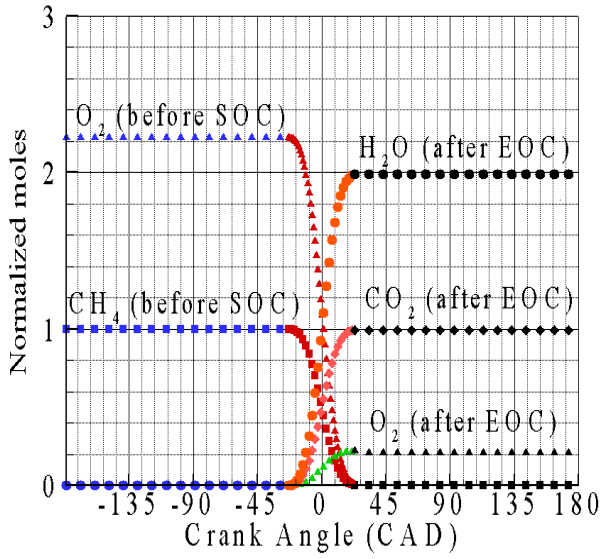

Figure 3: Temporal variation of CH_4, O_2, N_2, CO_2 and H_2O.

Figure 4 shows the temporal variation of NO concentration (in moles/m^3) using the simplified chemistry along with the equilibrium NO concentration in the burned zone.

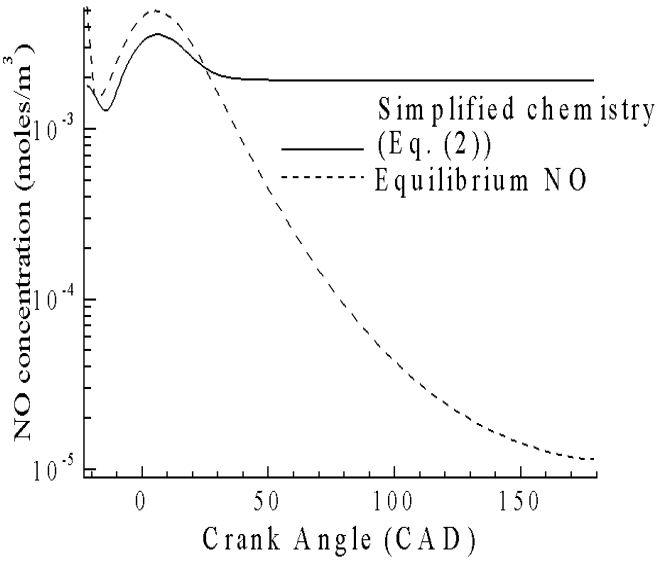

Figure 4: NO concentration obtained using the simplified chemistry and equilibrium chemistry

Following EOC, when the cylinder volume is increasing and the engine temperature and pressure are dropping, NO concentration predicted from equilibrium assumptions drops steeply. However, the NO concentration predicted using the simplified finite-rate kinetic model reaches steady state a few crank-angle degrees after EOC. It is instructive to understand

this behavior by a clogser examination of the RHS of Eq. (2). During the expansion process the drop in temperature and pressure leads to a sharp drop in k_1^+, and $[O]_e$. This is expected since k_1^+ depends strongly on temperature. Furthermore, lower temperatures yield lower $[O]_e$. Since the cylinder volume is also continuously increasing during the expansion stroke, the concentration of $[O]_e$ and $[N_2]_e$ (measured as moles/m^3) also drop on account of the increasing cylinder volume. The RHS of Eq. (2) is determined by R_1, N_1 and D_1. Beyond a crank angle of 50 ATDC, R_1 is on the order of 10^{-4} or less, while the ratio of N_1/D_1 in Eq. (2) is on the order of 10. Hence the overall numerical value of the RHS of Eq. (2) is on the order of 10^{-3} or less, implying no significant change in the temporal variation of NO concentration. However, this behavior is non-physical. The overall NO concentration has to drop during the expansion stroke, so that the total moles of NO (expressed as the product of NO concentration and instantaneous cylinder volume) remains nearly constant. This is on account of the fact that the NO formation process is practically frozen a few-crank angle degrees after EOC.

Figure 5 show the temporal variation of NO (in ppm) as a function of crank angle for the simplified chemistry and equilibrium chemistry cases.

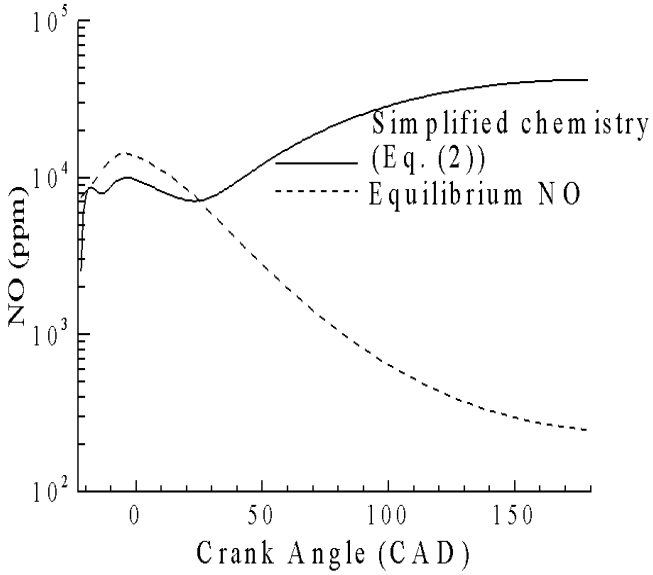

Figure 5: Temporal variation of NO (ppm) with simplified chemistry and equilibrium chemistry.

As explained above, the simplified chemistry model shows a monotonic increase in NO moles (expressed as ppm) and this increase follows the monotonic increase in the instantaneous cylinder volume during the expansion stroke. Based on above discussion, the simplified chemistry model does not capture the expected behavior of a monotonic decrease in the total concentration (moles/m^3) of NO. The results of the full finite-rate chemistry model are discussed next. Results shown in Figures 6 through 10 have been obtained using full finite-rate chemistry.

Figure 6 shows the temporal variation of nitrogen atoms (expressed as moles) obtained from the solution of Eq. (18). The reaction rate constants are computed using instantaneous temperatures obtained from the single-zone or two-zone model (as the case may be). It was assumed that the ratio of initial number of nitrogen atoms to nitrogen molecules at BDC was $2x10^{-5}$. The same ratio was also used for oxygen atoms and molecules at BDC. Before SOC, the N atoms (or moles) obtained from the single-zone and two-zone models are the same.

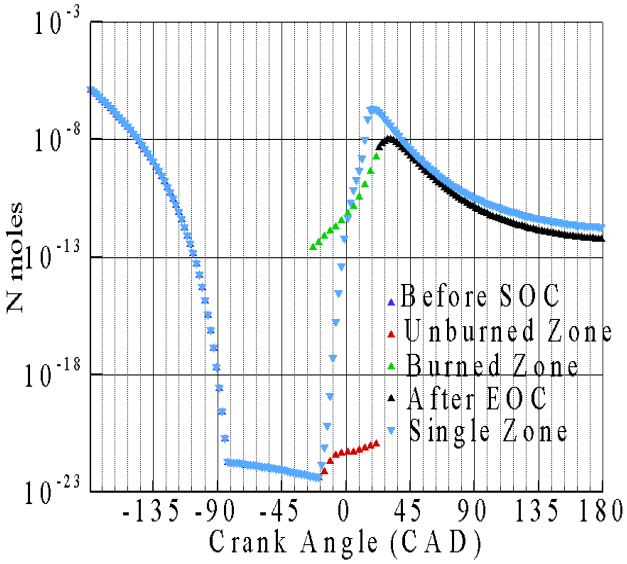

Figure 6: Temporal variation of N moles using single-zone and two-zone models.

This is to be expected as there temperature, pressure and mixture composition of the single zone and two-zone models are identical before SOC. The full-finite rate chemistry model predicts a sharp drop in the total moles of N due to recombination process. The net production of N atoms are determined by the source term based on the reaction mechanism showed in Table 2. Numerical evaluation of the source terms for formation of N atoms shows that the rate of depletion of N is strongly controlled by the forward reaction rate constant for reaction 2. Since reaction 2 has a relatively small activation energy (as compared to the forward reaction rate constant of reaction 1), there is a rapid depletion of N at low temperature (< 700 K). After SOC, the temperature of the unburned gas is still low (< 900K) and hence there is no appreciable rise in the formation of N atoms in this zone. The burnt zone however has a high temperature which supports the formation of N atoms rapidly as the burned volume increases. The rapid increase in the N atom population is aided by the increasing temperature and the presence of higher amounts of heated N_2. After EOC, when the cylinder temperature and pressure starts dropping with a simultaneous increase of

cylinder volume, the overall formation of N atoms starts to drop. The single-zone model exhibits a similar physical behavior. There is a sharp rise in N atom production from SOC to EOC followed by a drop during the expansion stroke. Figure 7 shows the temporal variation of O moles for the single-zone and two-zone models. Again, it is seen that there is a sharp increase in O atom formation during combustion (from SOC to EOC) followed by a drop during the expansion stroke. The full-finite rate chemistry model thus captures the physically expected behavior of N and O atom formation correctly during the entire engine cycle.

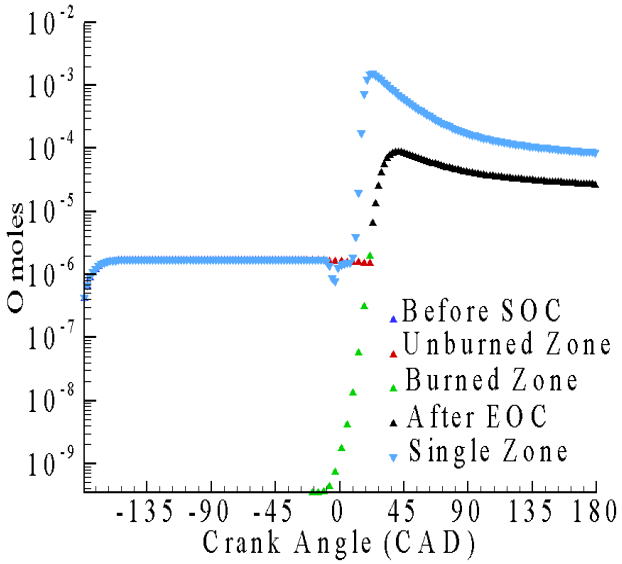

Figure 7: Temporal variation of O moles using single-zone and two-zone models.

Figure 8 shows the temporal variation of NO moles using the single-zone and two-zone models. It is seen that the full-finite chemistry model predicts a near constant value of NO moles after EOC. It is believed that the NO formation (in terms of total moles) freezes a few crank-angle degrees after EOC. The full finite-rate chemistry model correctly predicts this physically expected behavior. Figure 9 shows the temporal variation of NO concentration (expressed in moles/m^3) predicted by the full finite-rate chemistry model. As expected, the full finite-rate chemistry correctly predicts a drop in NO concentration, whereas the simplified chemistry model predicts the NO concentration to be constant after EOC (as shown in Figure 4).

The quantitative values of N, O and NO atoms predicted by the single-zone and two-zone models are different on account of the mixing assumption. In a single zone model, the number density of a particular species (say N, O, N_2 or O_2) is computed using all the moles of that particular specie present in the engine cylinder at that particular instant in the computation of the source term (RHS of Eq. (18)). The average cylinder temperature at that particular instant (crank angle) was used to compute the reaction rate constants. In the two-zone model, only the moles of a given specie in a given zone (either burned or unburned) was used to compute the number density along with the corresponding temperature of the zone in question.

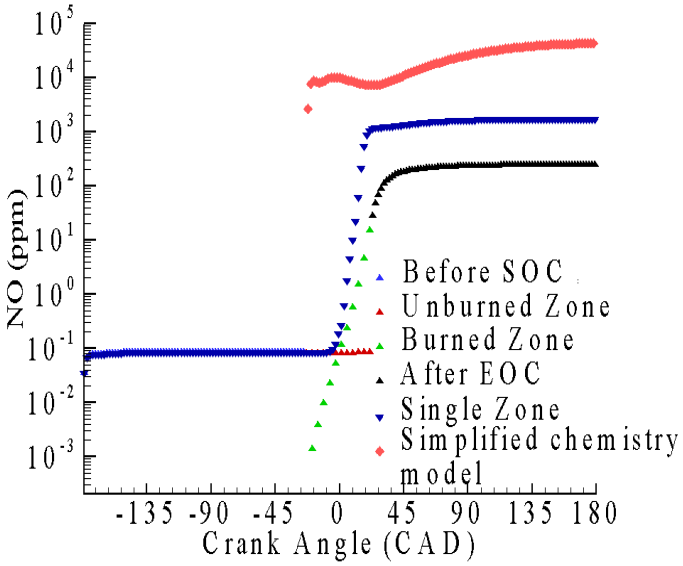

Figure 8: Temporal variation of NO moles using single-zone and two-zone models.

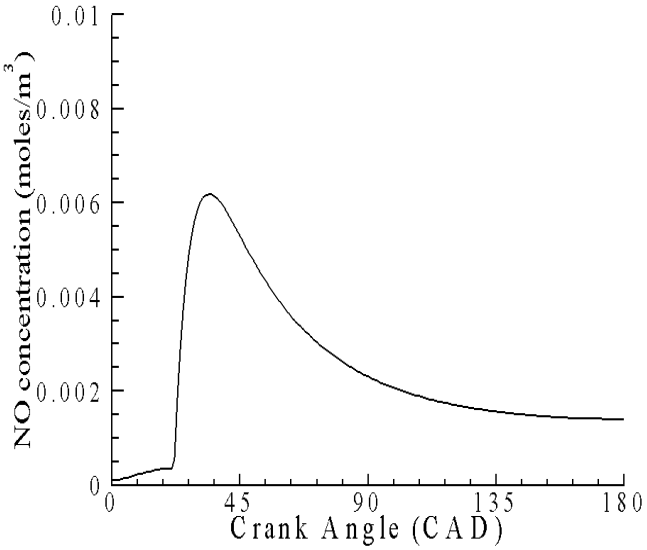

Figure 9: Temporal variation of NO concentration (moles/m^3) in a two-zone model using full finite-rate chemistry.

Figure 10 shows the temporal variation of N_2O moles. It is seen that the N_2O moles remains fairly constant after EOC. It is also seen that the N_2O moles are about 3 orders of magnitude lower than NO moles after EOC, as expected.

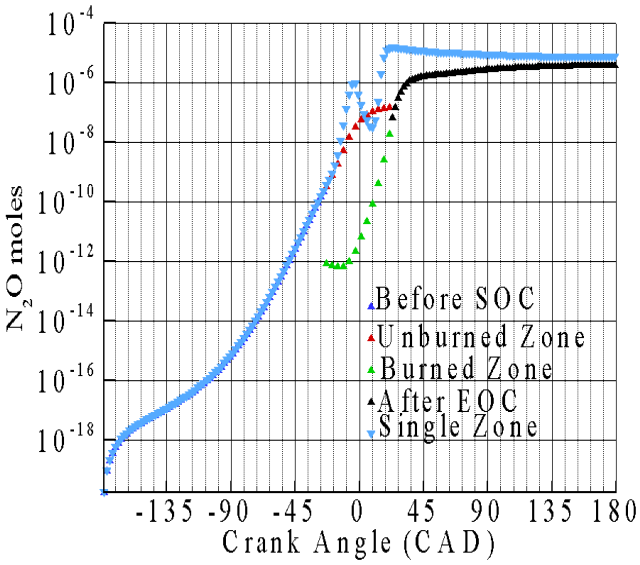

Figure 10: Temporal variation of N_2O moles using single-zone and two-zone models.

Short computational times is one of the main advantages of quasi-dimensional models over detailed CFD simulations. For instance, computation of the cylinder temperature, pressure and species concentrations (using full finite-rate chemistry) for the entire compression and expansion stroke takes about 0.75 seconds on a single CPU 2.53 GHz Intel processor for the two zone model. The two-zone model takes about 2.45 seconds. These short computational times make it feasible to conduct finite rate chemistry computations using more detailed NO_x and fuel combustion mechanisms in quasi-dimensional codes.

5 CONCLUSIONS

This work focused on comparing the traditional method of NO computations (simplified finite-rate chemistry) in quasi-dimensional engine codes with full finite rate chemistry. A single-zone and two-zone model was used to compute the temporal variation of temperature in a SI natural gas engine. NO computations were conducted for the simplified finite-rate chemistry and the full-finite rate chemistry using these temperature and pressure input. It was shown that the simplified finite-rate chemistry model does not accurately capture the physically expected behavior of NO formation, whereas the full finite-rate chemistry does so correctly.

ACKNOWLEDGMENTS

This work was supported in part by the U.S. Dept. of Energy under Contract DE-AC02-06CH11357.

REFERENCES

1. A. A. Abdel-Rahman, M. M. Osman, "Experimental investigation on varying the compression ratio of SI engine working under different ethanol-gasoline fuel blends. *Int. J. Energy Research* (21) 1997.
2. M. Al-Hasan, "Effect of ethanol–unleaded gasoline blends on engine performance and exhaust emission", *Energy Conversion and Management* 44 (2003) 1547–1561.
3. M A R S Al-Baghdadi, "Measurement and prediction study of the effect of ethanol blending on the performance and pollutants emission of a four-stroke spark ignition engine", Proc. IMechE Vol. 222 *Part D: J. Automobile Engineering* (2008).
4. M. Abu-Zaid, O. Badran and J. Yamin, "Effect of Methanol Addition on the Performance of Spark Ignition Engines", *Energy & Fuels* 2004, 18, 312-315.
5. D. Jung and D. N. Assanis, "Quasidimensional modeling of direct injection diesel engine nitric oxide, soot, and unburned hydrocarbon emissions", J. Eng. Gas Turbines Power, April 2006 Vol. 128(2), pp.388-396
6. S. Verhelst, R. Sierens, "A quasi-dimensional model for the power cycle of a hydrogen-fuelled ICE", Int. J. Hydrogen Energy, Vol. 32 (15), Oct. 2007, pp 3545–3554.
7. F. Tinaut, A. Melgar, A. Horrillo, "Utilization of a Quasi-Dimensional Model for Predicting Pollutant Emissions in SI Engines," SAE Technical Paper 1999-01-0223, 1999.
8. H. Li and G. A. Karim, " Hydrogen Fueled Spark-Ignition Engines Predictive and Experimental Performance", J. Eng. Gas Turbines Power, Jan. 2006, Vol. 128 (1) pp. 230-236.
9. S. M. Aithal, "Modeling of NO_x formation in diesel engines using finite-rate chemical kinetics", Applied Energy; 2010, Vol. 87(7), pp. 2256-2265.
10. F. Salimi, A. H. Shamekhi and A. M. Pourkhesalian, "Effects of Spark Advance, A/F Ratio and Valve Timing on Emission and Performance Characteristics of Hydrogen Internal Combustion Engine", SAE Technical Paper 2009-01-1424, 2009.
11. R. Egnell, "Combustion diagnostics by means of a multizone heat release analysis and NO calculation", *SAE 981424*.
12. M. Lapuerta, J. J. Hernández, O. Armas, "Kinetic modelling of gaseous emissions in a diesel engine", *SAE 2000-01-2939*.
13. M. Andersson, B. Johansson, A. Hultqvist, C. Nöhre, "A predictive real time NO_x model for conventional and partially premixed diesel combustion", SAE 2006-01-3329.
14. A. M. Mellor, J. P. Mello, K. P. Duffy, W. L. Easley and J. C. Faulkner, "Skeletal mechanism for NO_x chemistry in diesel engines", *SAE 98145*.
15. S. M. Aithal, "Equilibrium chemistry calculations for lean and rich hydrocarbon-air mixtures", Preprint ANL/MCS-P1825-0111, January 2011.
16. J. B. Heywood, "Internal Combustion Engine Fundamentals", McGraw-Hill: New York , 1988.

17. C. R. Ferguson, A. T. Kirkpatrick, "Internal Combustion Engines: Applied Thermosciences" 2nd Ed, John Wiley and Sons, NY, 2001.
18. S. M. Aithal, "Impact of EGR fraction on diesel engine performance considering heat loss and temperature-dependent properties of the working fluid", *Int. J. Energy Research*. 2008, **33,** 415-430.
19. Biruduganti M., Gupta S., Bihari, B., McConnell S., Sekar R. Air separation membranes – an alternative to EGR in large bore natural gas engines. ASME Internal Combustion Engine 2009 Spring technical conference paper ICES2009-76054, 2009.

The submitted manuscript has been created in part by UChicago Argonne, LLC as Operator of Argonne National Laboratory ("Argonne") under Contract No. DE-AC02-06CH11357 with the U.S. Department of Energy. The U.S. Government retains for itself, and others acting on its behalf, a paid-up, nonexclusive, irrevocable worldwide license in said article to reproduce, prepare derivative works, works, distribute copies to the public, and perform publicly and display publicly, by or on behalf of the Government. Argonne, a U.S. Department of Energy Office of Science laboratory, is operated under Contract No. DE-AC02-06CH113.